Higher-order topology and fractional charge in monolayer graphene

Feng Liu [1,2,*] and Katsunori Wakabayashi [3,4,†]

[1]*School of Physical Science and Technology, Ningbo University, Ningbo 315-211, China*

[2]*Institute of High Pressure Physics, Ningbo University, Ningbo, 315-211, China*

[3]*Department of Nanotechnology for Sustainable Energy, School of Science and Technology, Kwansei Gakuin University, Gakuen 2-1, Sanda 669-1337, Japan*

[4]*Center for Spintronics Research Network (CSRN), Osaka University, Toyonaka 560-8531, Japan*

(Received 4 November 2020; accepted 20 April 2021; published 14 May 2021)

Typical higher-order topological systems require the fine-tuning of hopping textures and external fields, which considerably hinders their practical realization. Based on a simple picture that corners are "edges" of edges, we determine that in the already-thoroughly-studied monolayer graphene, higher-order topological corner states appear without introducing any additional effects. Unlike quadrupole insulators, owing to degenerate Dirac points in graphene, the emergence of topological corner states depends on the corner angle and edge geometries. We provide a useful expression for the indication of corner states in graphene by the product of Zak phases. We also discuss the methods for experimental detection of the nontrivial higher-order topology in graphene such as the fractional corner anomaly and the disparity of local density of states between trivial and nontrivial corners.

DOI: 10.1103/PhysRevResearch.3.023121

The topology of energy bands offers us a new dimension of designing solid-state materials with intriguing properties [1–3]. One of the essential properties of topologically nontrivial systems is the bulk-edge correspondence, where robust edge and surface states appear at the interfaces that separate two topologically distinct systems [4,5]. These topological states are insensitive to local perturbations that preserve bulk topological invariants, which is also called topological protection. The recently proposed higher-order topology has extended such bulk-edge correspondence to the more general bulk-edge-corner correspondence, where the topological states of codimension larger than 1, i.e., topological corner states in two-dimensional systems, appear [6,7]. The higher-order topology has attracted considerable attention in condensed matter physics owing to its fundamental scientific importance and also because of its potential applications in electronics. In particular, topological corner states allow us to design laser cavity and quantum computation with topological protection and maximized efficiency [8–11].

Based on several prototype models of higher-order topology (e.g., the two-dimensional Su-Schrieffer-Heeger model, quadrupole insulator, and breathing kagome lattice), nontrivial higher-order topology usually requires the fine-tuning of hopping textures and external fields [12–14]. Along this line, several proposals (e.g., monolayer graphdiyne [15], Kekulé-like lattice [16], twisted bilayer graphene [17], and topological insulators with the breaking of time-reversal symmetry [18,19]) have been created. Unfortunately, the fine-tuning of hopping textures is difficult to realize in solid-state materials, owing to difficulties in the precise control of crystal growth. In addition to the observation of topological corner states in several artificial crystalline structures [20–29], the realization of higher-order topological states remains elusive in solid-state materials, especially in two-dimensional materials.

Without the fine-tuning of hopping textures or applying external fields, it is hard to imagine the emergence of higher-order topological states, especially in uniform systems. Motivated by a simple picture that corners are "edges" of edges, we consider monolayer graphene as a possible candidate for topological corner states. This occurs because in graphene, topological edge states accompanied with the perfectly conducting channel appear for various geometric ribbons only except for the armchair edge [30,31]. Later, it has been shown that the emergence of these edge states in graphene is due to a nonzero geometric phase—the Zak phase [32]. The Zak phase is a topological indicator for systems of zero Chern number that corresponds to the bulk charge polarization [33–37]. Under several crystalline symmetries such as inversion symmetry, point group symmetries, and the chiral symmetry, the Zak phase is quantized, which suggests that the Zak-phase type of higher-order topological insulators is a particular class of topological crystalline insulators [38–48]. Finite bulk charge polarization casts fractional surface charge in the direction perpendicular to the edges and results in topological edge states [34]. When the Zak phases in graphene are along the two directions, those that are perpendicular to the edges forming the corner are both nontrivial; thus, a corner state emerges.

*Liufeng@nbu.edu.cn

†waka@kwansei.ac.jp

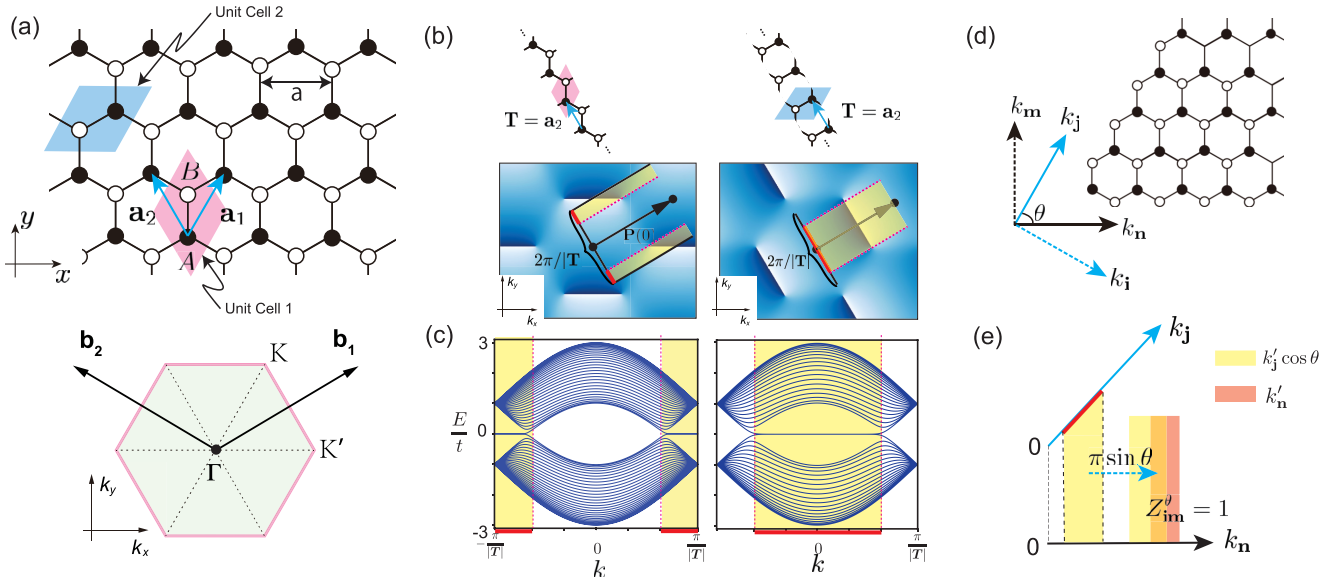

FIG. 1. (a) Top: Schematic of monolayer graphene with the primitive lattice vectors $\mathbf{a}_1 = a(1/2, \sqrt{3}/2)$ and $\mathbf{a}_2 = a(-1/2, \sqrt{3}/2)$. a is the lattice constant of graphene. There are two choices of unit cells, which are indicated by shaded rhombuses. Magenta and cyan rhombuses are called unit cells 1 and 2, respectively. Bottom: First Brillouin zone (shaded hexagonal region) with the reciprocal primitive vectors $\mathbf{b}_1 = \frac{2\pi}{a}(1, 1/\sqrt{3})$ and $\mathbf{b}_2 = \frac{2\pi}{a}(-1, 1/\sqrt{3})$. The coordinates of high symmetric points are $\mathbf{\Gamma} = (0, 0)$, $\mathbf{K} = \frac{2\pi}{a}(\frac{1}{3}, \frac{1}{\sqrt{3}})$, and $\mathbf{K}' = \frac{2\pi}{a}(\frac{4}{3}, 0)$. (b) Bottom panels: Density plots of $\phi(\mathbf{k})$ in the momentum space for the unit cells I (left) and II (right), where black circles indicate the Γ point. For zigzag and bearded ribbons with the period of $\mathbf{T} = \mathbf{a}_2$, $\mathcal{Z}(k) = \pi$ when the path $\mathbf{P}(k)$ passes through the discontinuities of $\phi(\mathbf{k})$, as indicated by yellow. The upper structures show the unit cells of (left) zigzag and (right) bearded ribbons, which are produced by repeating the unit cells I and II with $\mathbf{T} = \mathbf{a}_2$, respectively. (c) Energy band structure for the zigzag graphene ribbon (left) and bearded graphene ribbon (right), where the range has a nontrivial topological phase (indicated by yellow). The range is k', which is $[-\pi, -2\pi/3) \cup (2\pi/3, \pi]$ for the zigzag ribbon and $[-2\pi/3, 2\pi/3]$ for the bearded ribbon. The width of zigzag and bearded ribbons is set to $15\sqrt{3}a$ for the calculation of energy band structures. (d) Graphene corner with angle θ formed by two edges along $k_\mathbf{j}$ and $k_\mathbf{n}$, where $k_\mathbf{i}$ and $k_\mathbf{m}$ are perpendicular to $k_\mathbf{j}$ and $k_\mathbf{n}$, respectively. The corner state appears when an imaginary solution of $\mathbf{k}$ along both $\mathbf{i}$ and $\mathbf{m}$ exists. (e) Schematic of the corner states indicator $Z^\theta_{\mathbf{im}}$ in graphene. An imaginary solution of $\mathbf{k}$ along $\mathbf{i}$ and $\mathbf{m}$ exists when both $k_\mathbf{j}$ and $k_\mathbf{n}$ are in their corresponding nontrivial ranges $k'_\mathbf{j}$ and $k'_\mathbf{n}$. Following the relation that $k_\mathbf{n} = \pi \sin\theta + k_\mathbf{j} \cos\theta$, the above-mentioned condition can be fulfilled when there is an overlap between the range $k'_\mathbf{j}\cos\theta + \pi \sin\theta$ and $k'_\mathbf{n}$.

In monolayer graphene, the geometries of edges (ribbons) can be characterized by a chosen unit cell with the period $\mathbf{T} = m\mathbf{a}_1 + n\mathbf{a}_2$ [31,32]. Here, $\mathbf{a}_1$ and $\mathbf{a}_2$ are the primitive lattice vectors of graphene, as shown on the upper panel of Fig. 1(a),and m, n are coprime. We set $|\mathbf{T}| = 1$ for later discussions. For example, we obtain a zigzag (bearded) ribbon by repeating the unit cell I (II) shown in Fig. 1(a) with $T = \mathbf{a}_2$. The nontrivial Zak phase in graphene originates from the degenerate Dirac points at K and K' in the first Brillouin zone, as shown on the lower panel of Fig. 1(a), where $\mathbf{b}_1$ and $\mathbf{b}_2$ are the reciprocal lattice vectors. These Dirac points in graphene can be described well by the tight-binding model with nearest-neighbor hopping, i.e., $H(\mathbf{k}) = \mathrm{Re}(\rho)\sigma_x + \mathrm{Im}(\rho)\sigma_y$ with $\rho \equiv |\rho| e^{-i\phi(\mathbf{k})}$ and σ_i Pauli matrix [49]. The bulk topology of graphene is encoded in $\phi(\mathbf{k})$. For the ribbon with period $\mathbf{T}$, its Zak phase is given by the winding of ϕ along $\mathbf{P}(k)$ as $Z_\mathbf{i}(k) = \frac{1}{2\pi}\int_{\mathbf{P}(k)} d\phi(\mathbf{k})$, where $\mathbf{P}$ in the direction $\mathbf{i}$ is a straight path that is perpendicular to $\mathbf{T}$ and $\mathbf{P} \times \mathbf{T} = \mathbf{b}_1 \times \mathbf{b}_2$ [32]. Of note, for different choices of the unit cell, ϕ changes correspondingly. Because of the chiral symmetry, $Z_\mathbf{i}(k)$ is either 1 or zero in graphene and thus serves as a topological indicator. Figure 1(b) shows the density plots of $\phi(\mathbf{k})$ for zigzag and bearded ribbons, respectively. Figure 1(b) shows that when $\phi(\mathbf{k})$ passes through the discontinuities along $\mathbf{P}(k)$, $Z_\mathbf{i}(i)$ is nontrivial, and edge states appear at the corresponding k in their energy band structures, as shown in Fig. 1(c). For the nontrivial k range, we mark them as k'. For k in k', an imaginary wavenumber solution $k_\mathbf{i} = \pi + i\eta_\mathbf{i}$ along $\mathbf{i}$ exists for the boundary condition, e.g., $\sin(k_\mathbf{i}N) + 2\cos(k/2)\sin[k_\mathbf{i}(N+1)] = 0$ of a width-N zigzag ribbon, where $\eta_\mathbf{i}$ is the inverse of the localization length of the edge state [32,50]. For the emergence of corner states, an imaginary wave-vector solution $\mathbf{k}$ is required. This condition is fulfilled if $Z_\mathbf{i}(k_\mathbf{j})$ and $Z_\mathbf{m}(k_\mathbf{n})$ are both nontrivial. Unlike higher-order topological insulators, in graphene $Z_\mathbf{i}(k_\mathbf{j})$ and $Z_\mathbf{m}(k_\mathbf{n})$ are not independent, as Dirac points separate the wavenumber space into several topologically distinct areas as shown in Figs. 1(b) and 1(c), and $\mathbf{j}$, $\mathbf{n}$ are also not orthogonal. Here, $\mathbf{j}$ and $\mathbf{n}$ are directions paralleling edges forming the corner of angle $\theta \in [0, \pi)$, and $\mathbf{i}$, $\mathbf{m}$ are the corresponding orthogonal directions, as shown in Fig. 1(d). Following the simple picture that a corner is the "edgeof an edge," we assume $Z_\mathbf{i}(k_\mathbf{j})$ is nontrivial without loss of generality, and have the relation that $k_\mathbf{n} = \pi \sin\theta + k'_\mathbf{j}\cos\theta$ as suggested in Fig. 1(d). When $k_\mathbf{n} \in k'_\mathbf{n}$, an imaginary $\mathbf{k}$ along both $\mathbf{i}$ and $\mathbf{n}$ exists. In a compact form, the indicator of graphene corner

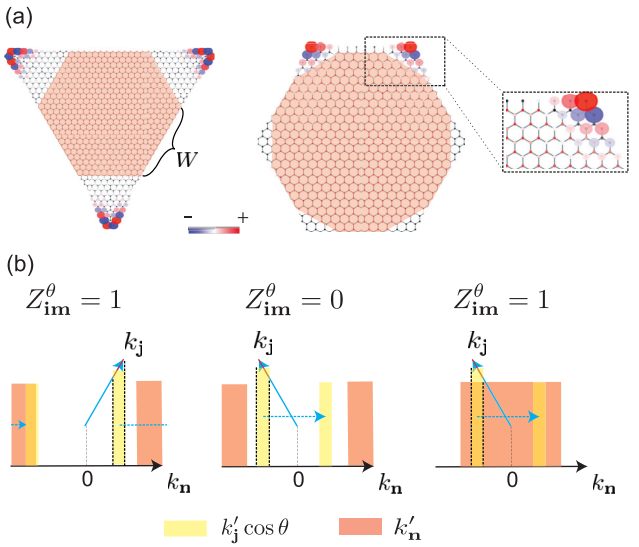

FIG. 2. (a) Topological corner states appear in the $\pi/6$ zigzag-zigzag corner and in the $\pi/3$ zigzag-bearded corner and are absent in the $\pi/3$ zigzag-zigzag corner. The size of circles indicates the local amplitude of the wavefunction, and blue and red are their signs. The red in the middle parts is the non-Hermitian mask where an imaginary on-site potential $-0.005t$ is assumed. The inset shows a magnified view of the topological corner state in the $\pi/3$ zigzag-bearded corner. (b) Graphic representations of Z^{θ}_{im} for three types of corners in (a). From left to right, they are for the $\pi/6$ zigzag-zigzag corner, $\pi/3$ zigzag-zigzag corner, and zigzag-bearded corner, respectively.

states can be presented as

$$Z^{\theta}_{\mathrm{im}} = \bigvee_{k_{\mathrm{j}}>0} Z_{\mathrm{i}}(k_{\mathrm{j}}) Z_{\mathrm{m}}(k_{\mathrm{j}}\cos\theta + \pi\sin\theta), \tag{1}$$

where $\bigvee_{k_{\mathrm{j}}>0}$ is the logical "or" for all possible $k_j > 0$ within the first Brillouin zone. Figure 1(e) is the graphic explanation of Eq. (1), where if the projection of k'_{j} on $\mathbf{n}$ after a $\pi\sin\theta$ shift overlaps with k'_{n}, Z^{θ}_{im} is nontrivial. Of note, Z^{θ}_{im} and Z^{θ}_{mi} are not equivalent in general; only when neither of them is nontrivial, the corner state is absent. Equation (1) reduces to the product of Zak phases in higher-order topological insulators. Different from previously studied topological quadrupolar semimetals [51–59], the nontrivial higher-order topology in graphene originates from Dirac points protected by the chiral symmetry and we dub this type of higher-order topological semimetal a higher-order topological Dirac semimetal.

To demonstrate Eq. (1), we use the zigzag-zigzag corner as an example. There are two possible angles for the zigzag-zigzag corners, which are $\pi/3$ and $\pi/6$ [60,61]. Topological corner states appear in the $\pi/6$ zigzag-zigzag corners and are absent in the $\pi/3$ corners, as shown in Fig. 2(a). By replacing one zigzag edge with the bearded edge in the $\pi/3$ zigzag-zigzag corner, the topological corner state reappears in the $\pi/3$ zigzag-bearded corner, as shown on the right of Fig. 2(a). Such appearance and disappearance of corner states in various geometric edges and corner angles shown in Fig. 2(a) can be characterized well by Z^{θ}_{im}. Figure 2(b) graphically shows the indicator Z^{θ}_{im} for these three types of corners: from left to right

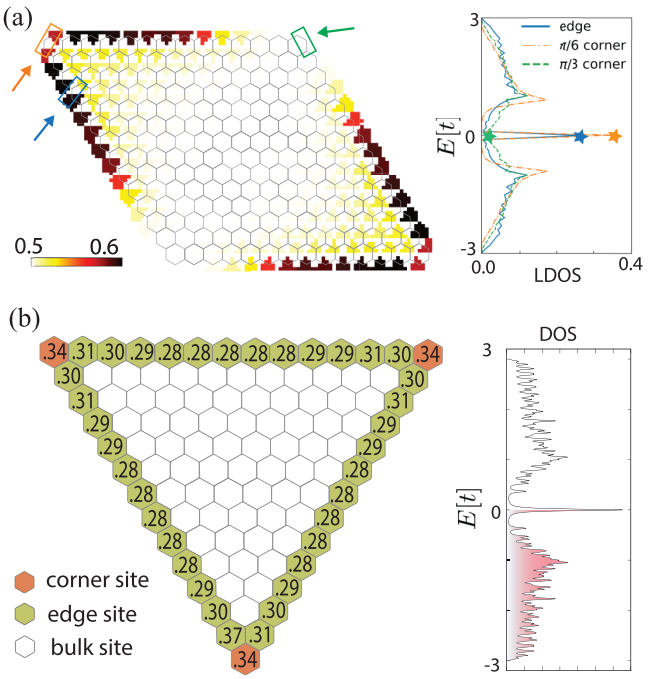

FIG. 3. (a) Left: Integrated density of states of a graphene sample with both $\pi/6$ and $\pi/3$ zigzag-zigzag corners over $E \leqslant 0$. Right: Local density of states spectrum located at edge, and $\pi/6$ and $\pi/3$ zigzag-zigzag corners, which are indicated by the arrows in left panel. The stars mark the maxima at zero energy. (b) Left: Fractional corner anomaly for the C_3-symmetric graphene sample at the half-filling case. The fraction of total state density considering spin degeneracy in each hexagonal cell is shown in purple with white text. Right: Density of states spectrum for the C_3-symmetric graphene sample, where the color indicates the half-filling case.

they are are Z^{θ}_{im} for the $\pi/6$ zigzag-zigzag corner, $\pi/3$ zigzag-zigzag corner, and $\pi/3$ zigzag-bearded corner, respectively. Because of the opposite projection directions, Z^{θ}_{im} is nontrivial in the $\pi/6$ zigzag-zigzag corner and trivial in the $\pi/3$ zigzag-zigzag corner. The topological corner state reappears in the $\pi/3$ zigzag-bearded corner because the bearded ribbon has a complementary k' range compared to the zigzag ribbon.

For experimental detection of the nontrivial higher-order topology in graphene, we may use the scanning tunneling microscope [62–64]. As displayed on the left of Fig. 3(a), the nontrivial second-order topology in graphene manifests as stronger density of states at paired edges that form the corner. Furthermore, there also exists an obvious disparity of local density of states at zero energy among nontrivial corner and trivial corner sites, as displayed on the right of Fig. 3(a). Besides density of states signals, there is also a fractional corner anomaly in the C_3-symmetric sample shown in Fig. 2(a) [65]. As displayed in left of Fig. 3(b), we have the fractional corner anomaly

$$\phi = \rho - (\sigma_1 + \sigma_2) = 0.34 - 7.04 = 0.3 \approx \tfrac{1}{3}, \tag{2}$$

considering the spin degeneracy with ρ and σ_i the corner and edge sites densities. This fractional corner charge reveals the nontriviality of higher-order topology in graphene. The right

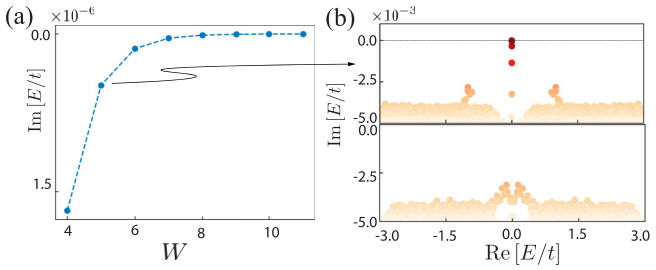

FIG. 4. (a) Dependence of the imaginary part of eigenenergy for the topological corner state in the $\pi/6$ zigzag-zigzag corner on the non-Hermitian mask size W. By increasing the size of the non-Hermitian mask, the imaginary part of the eigenenergy of the topological corner state in the $\pi/6$ zigzag-zigzag corner exponentially approaches zero. (b) Complex energy spectra of the $\pi/6$ zigzag-zigzag corner sample with the non-Hermitian mask size $W = 5$ and $\pi/3$ zigzag-zigzag corner sample.

of Fig. 3(b) displays the density-of-states spectrum of the C_3-symmetric graphene sample of half filling.

For metallic systems, in general, the localized corner state is buried in the bulk and edge states, which is also called a bound state in continuum [66,67]. To pick the corner states out, we use a non-Hermitian mask [67,68], i.e., an imaginary on-site potential $\alpha = -0.005t$, which is indicted by the red shading in Fig. 2(a). In practice, the non-Hermitian part presents the coupling with the environment, which can be realized by the temperature control of the sample [68–70]. Using such a non-Hermitian mask, only topological corner states remain nondecayed, while the bulk and edge states fade out owing to the localization nature of corner states. As shown in Fig. 4(a), the decaying rate of the topological corner state in the $\pi/6$ zigzag-zigzag corner exponentially approaches zero by increasing the area of the non-Hermitian mask. From the complex energy spectrum of the $\pi/6$ zigzag-zigzag corner sample [upper panel in Fig. 4(b)], we see that, except for the topological corner states, all other eigenstates have finite decaying rates. In the $\pi/3$ zigzag-zigzag corner sample, there is no nondecayed state owing to the absence of topological corner states [lower panel in Fig. 4(b)].

Finally, we mention that the emergence of topological corner states in graphene is due to the nontrivial Zak phases along two nonparallel directions. The perturbations that break the chiral symmetry only conceptually break the topological protection and cannot completely suppress the corner states [71]. The large spin-orbit coupling destroys the topological corner states in graphene, because a finite Chern number for a single spin channel breaks the monodromy of the Zak phase [72,73]. It is fortunate that spin-orbit couplings are minimal in graphene, and we can safely neglect them.

To summarize, we studied the higher-order topology of monolayer graphene. We determined that topological corner states exist in graphene for various geometric boundaries and corner angles. These topological corner states in graphene correspond to a twisted higher-order topological structure associated with the product of Zak phases in momentum space. Our results provide a possible way of intrinsically localizing electrons within atomic sizes with the topological protection in metallic systems, and also yields a platform for detecting fractional charge in electronic solid-state systems. Our predication is only based on monolayer graphene without substrate effects and spin-orbit couplings; we believe that the experimental observation of topological corner states in graphene is possible through the proposed methods.

ACKNOWLEDGMENTS

This work is supported by the Research Starting Funding of Ningbo University and NSFC Grant No. 12074205. K.W. acknowledges the financial support by JSPS KAKENHI (Grants No. JP21H01019 and No. JP18H01154) and JST CREST (Grant No. JPMJCR19T1).

[1] M. Z. Hasan and C. L. Kane, Colloquium: Topological insulators, Rev. Mod. Phys. **82**, 3045 (2010).
[2] X.-L. Qi and S.-C. Zhang, Topological insulators and superconductors, Rev. Mod. Phys. **83**, 1057 (2011).
[3] A. Bansil, H. Lin, and T. Das, Colloquium: Topological band theory, Rev. Mod. Phys. **88**, 021004 (2016).
[4] Y. Hatsugai, Chern Number and Edge States in the Integer Quantum Hall Effect, Phys. Rev. Lett. **71**, 3697 (1993).
[5] D. N. Sheng, Z. Y. Weng, L. Sheng, and F. D. M. Haldane, Quantum Spin-Hall Effect and Topologically Invariant Chern Numbers, Phys. Rev. Lett. **97**, 036808 (2006).
[6] W. A. Benalcazar, B. A. Bernevig, and T. L. Hughes, Quantized electric multipole insulators, Science **357**, 61 (2017).
[7] Z. Song, Z. Fang, and C. Fang, $(d-2)$-Dimensional Edge States of Rotation Symmetry Protected Topological States, Phys. Rev. Lett. **119**, 246402 (2017).
[8] G. Harari, M. A. Bandres, Y. Lumer, M. C. Rechtsman, Y. D. Chong, M. Khajavikhan, D. N. Christodoulides, and M. Segev, Topological insulator laser: Theory, Science **359**, eaar4003 (2018).
[9] W. Zhang, X. Xie, H. Hao, J. Dang, S. Xiao, S. Shi, H. Ni, Z. Niu, C. Wang, K. Jin, X. Zhang, and X. Xu, Low-threshold topological nanolasers based on the second-order corner state, Light Sci. Appl. **9**, 109 (2020).
[10] Y. Wu, H. Liu, J. Liu, H. Jiang, and X. C. Xie, Double-frequency Aharonov-Bohm effect and non-Abelian braiding properties of Jackiw-Rebbi zero-mode, Natl. Sci. Rev. **7**, 572 (2019).
[11] Y. Wu, H. Jiang, J. Liu, H. Liu, and X. C. Xie, Non-Abelian Braiding of Dirac Fermionic Modes Using Topological Corner States in Higher-Order Topological Insulator, Phys. Rev. Lett. **125**, 036801 (2020).
[12] F. Liu and K. Wakabayashi, Novel Topological Phase with a Zero Berry Curvature, Phys. Rev. Lett. **118**, 076803 (2017).
[13] W. A. Benalcazar, B. A. Bernevig, and T. L. Hughes, Electric multipole moments, topological multipole moment pumping, and chiral hinge states in crystalline insulators, Phys. Rev. B **96**, 245115 (2017).
[14] M. Ezawa, Higher-Order Topological Insulators and Semimetals on the Breathing Kagome and Pyrochlore Lattices, Phys. Rev. Lett. **120**, 026801 (2018).

[15] B. Liu, G. Zhao, Z. Liu, and Z. F. Wang, Two-dimensional quadrupole topological insulator in γ-graphyne, Nano Lett. **19**, 6492 (2019).

[16] F. Liu, H.-Y. Deng, and K. Wakabayashi, Helical Topological Edge States in a Quadrupole Phase, Phys. Rev. Lett. **122**, 086804 (2019).

[17] M. J. Park, Y. Kim, G. Y. Cho, and S. B. Lee, Higher-Order Topological Insulator in Twisted Bilayer Graphene, Phys. Rev. Lett. **123**, 216803 (2019).

[18] A. Matsugatani and H. Watanabe, Connecting higher-order topological insulators to lower-dimensional topological insulators, Phys. Rev. B **98**, 205129 (2018).

[19] Y. Ren, Z. Qiao, and Q. Niu, Engineering Corner States from Two-Dimensional Topological Insulators, Phys. Rev. Lett. **124**, 166804 (2020).

[20] M. Serra-Garcia, V. Peri, R. Süsstrunk, O. R. Bilal, T. Larsen, L. G. Villanueva, and S. D. Huber, Observation of a phononic quadrupole topological insulator, Nature (London) **555**, 342 (2018).

[21] C. W. Peterson, W. A. Benalcazar, T. L. Hughes, and G. Bahl, A quantized microwave quadrupole insulator with topologically protected corner states, Nature (London) **555**, 346 (2018).

[22] S. Imhof, C. Berger, F. Bayer, J. Brehm, L. W. Molenkamp, T. Kiessling, F. Schindler, C. H. Lee, M. Greiter, T. Neupert, and R. Thomale, Topolectrical-circuit realization of topological corner modes, Nat. Phys. **14**, 925 (2018).

[23] Y. Ota, F. Liu, R. Katsumi, K. Watanabe, K. Wakabayashi, Y. Arakawa, and S. Iwamoto, Photonic crystal nanocavity based on a topological corner state, Optica **6**, 786 (2019).

[24] X.-D. Chen, W.-M. Deng, F.-L. Shi, F.-L. Zhao, M. Chen, and J.-W. Dong, Direct Observation of Corner States in Second-Order Topological Photonic Crystal Slabs, Phys. Rev. Lett. **122**, 233902 (2019).

[25] H. Xue, Y. Yang, G. Liu, F. Gao, Y. Chong, and B. Zhang, Realization of an Acoustic Third-Order Topological Insulator, Phys. Rev. Lett. **122**, 244301 (2019).

[26] H. Xue, Y. Ge, H.-X. Sun, Q. Wang, D. Jia, Y.-J. Guan, S.-Q. Yuan, Y. Chong, and B. Zhang, Observation of an acoustic octupole topological insulator, Nat. Commun. **11**, 2442 (2020).

[27] B. Xie, G. Su, H.-F. Wang, F. Liu, L. Hu, S.-Y. Yu, P. Zhan, M.-H. Lu, Z. Wang, and Y.-F. Chen, Higher-order quantum spin Hall effect in a photonic crystal, Nat. Commun. **11**, 3768 (2020).

[28] Z. Xiong, Z.-K. Lin, H.-X. Wang, X. Zhang, M.-H. Lu, Y.-F. Chen, and J.-H. Jiang, Corner states and topological transitions in two-dimensional higher-order topological sonic crystals with inversion symmetry, Phys. Rev. B **102**, 125144 (2020).

[29] M. Kim, Z. Jacob, and J. Rho, Recent advances in 2D, 3D and higher-order topological photonics, Light Sci. Appl. **9**, 130 (2020).

[30] K. Wakabayashi, Y. Takane, M. Yamamoto, and M. Sigrist, Edge effect on electronic transport properties of graphene nanoribbons and presence of perfectly conducting channel, Carbon **47**, 124 (2009).

[31] A. R. Akhmerov and C. W. J. Beenakker, Boundary conditions for Dirac fermions on a terminated honeycomb lattice, Phys. Rev. B **77**, 085423 (2008).

[32] P. Delplace, D. Ullmo, and G. Montambaux, Zak phase and the existence of edge states in graphene, Phys. Rev. B **84**, 195452 (2011).

[33] J. Zak, Berry's Phase for Energy Bands in Solids, Phys. Rev. Lett. **62**, 2747 (1989).

[34] D. Vanderbilt and R. D. King-Smith, Electric polarization as a bulk quantity and its relation to surface charge, Phys. Rev. B **48**, 4442 (1993).

[35] D. Obana, F. Liu, and K. Wakabayashi, Topological edge states in the Su-Schrieffer-Heeger model, Phys. Rev. B **100**, 075437 (2019).

[36] H. C. Wu, L. Jin, and Z. Song, Nontrivial topological phase with a zero Chern number, Phys. Rev. B **102**, 035145 (2020).

[37] Y.-B. Yang, K. Li, L.-M. Duan, and Y. Xu, Type-II quadrupole topological insulators, Phys. Rev. Research **2**, 033029 (2020).

[38] L. Fu, C. L. Kane, and E. J. Mele, Topological Insulators in Three Dimensions, Phys. Rev. Lett. **98**, 106803 (2007).

[39] C. Fang, M. J. Gilbert, and B. A. Bernevig, Bulk topological invariants in noninteracting point group symmetric insulators, Phys. Rev. B **86**, 115112 (2012).

[40] Q.-F. Liang, J. Zhou, R. Yu, Z. Wang, and H. Weng, Node-surface and node-line fermions from nonsymmorphic lattice symmetries, Phys. Rev. B **93**, 085427 (2016).

[41] T. Kariyado, T. Morimoto, and Y. Hatsugai, Z_N Berry Phases in Symmetry Protected Topological Phases, Phys. Rev. Lett. **120**, 247202 (2018).

[42] F. Schindler, Z. Wang, M. G. Vergniory, A. M. Cook, A. Murani, S. Sengupta, A. Y. Kasumov, R. Deblock, S. Jeon, I. Drozdov, H. Bouchiat, S. Guéron, A. Yazdani, B. A. Bernevig, and T. Neupert, Higher-order topology in bismuth, Nat. Phys. **14**, 918 (2018).

[43] Y. Hwang, J. Ahn, and B.-J. Yang, Fragile topology protected by inversion symmetry: Diagnosis, bulk-boundary correspondence, and Wilson loop, Phys. Rev. B **100**, 205126 (2019).

[44] R. Okugawa, S. Hayashi, and T. Nakanishi, Second-order topological phases protected by chiral symmetry, Phys. Rev. B **100**, 235302 (2019).

[45] E. Cornfeld and A. Chapman, Classification of crystalline topological insulators and superconductors with point group symmetries, Phys. Rev. B **99**, 075105 (2019).

[46] A. Yoshida, Y. Otaki, R. Otaki, and T. Fukui, Edge states, corner states, and flat bands in a two-dimensional $\mathcal{PT}$-symmetric system, Phys. Rev. B **100**, 125125 (2019).

[47] Z.-D. Song, L. Elcoro, and B. A. Bernevig, Twisted bulk-boundary correspondence of fragile topology, Science **367**, 794 (2020).

[48] Z. Song, C. Fang, and Y. Qi, Real-space recipes for general topological crystalline states, Nat. Commun. **11**, 4197 (2020).

[49] $\rho_I = t(1 + e^{-i\mathbf{k}\cdot\mathbf{a}_1} + e^{-i\mathbf{k}\cdot\mathbf{a}_2})$ for unit cell 1, and $\rho_{II} = e^{i\mathbf{k}\cdot\mathbf{a}_1}\rho_I$ for unit cell 2. $t = 2.75$ eV in graphene.

[50] K. Wakabayashi, K. Sasaki, T. Nakanishi, and T. Enoki, Electronic states of graphene nanoribbons and analytical solutions, Sci. Technol. Adv. **11**, 054504 (2010).

[51] M. Lin and T. L. Hughes, Topological quadrupolar semimetals, Phys. Rev. B **98**, 241103(R) (2018).

[52] Z. Wang, B. J. Wieder, J. Li, B. Yan, and B. A. Bernevig, Higher-Order Topology, Monopole Nodal Lines, and the Origin of Large Fermi Arcs in Transition Metal Dichalcogenides $x\mathrm{Te}_2$ (x = Mo, W), Phys. Rev. Lett. **123**, 186401 (2019).

[53] M. Ezawa, Second-order topological insulators and loop-nodal semimetals in transition metal dichalcogenides $x\mathrm{Te}_2$ (x = Mo, W), Sci. Rep. **9**, 5286 (2019).

[54] X.-W. Luo and C. Zhang, Higher-Order Topological Corner States Induced by Gain and Loss, Phys. Rev. Lett. **123**, 073601 (2019).

[55] A. L. Szabó and B. Roy, Dirty higher-order Dirac semimetal: Quantum criticality and bulk-boundary correspondence, Phys. Rev. Research **2**, 043197 (2020).

[56] H.-X. Wang, Z.-K. Lin, B. Jiang, G.-Y. Guo, and J.-H. Jiang, Higher-Order Weyl Semimetals, Phys. Rev. Lett. **125**, 146401 (2020).

[57] B. J. Wieder, Z. Wang, J. Cano, X. Dai, L. M. Schoop, B. Bradlyn, and B. A. Bernevig, Strong and fragile topological Dirac semimetals with higher-order Fermi arcs, Nat. Commun. **11**, 627 (2020).

[58] Q.-B. Zeng, Y.-B. Yang, and Y. Xu, Higher-order topological insulators and semimetals in generalized Aubry-André-Harper models, Phys. Rev. B **101**, 241104(R) (2020).

[59] S. A. A. Ghorashi, T. Li, and T. L. Hughes, Higher-Order Weyl Semimetals, Phys. Rev. Lett. **125**, 266804 (2020).

[60] Y. Shimomura, Y. Takane, and K. Wakabayashi, Electronic states and local density of states in graphene with a corner edge structure, J. Phys. Soc. Jpn. **80**, 054710 (2011).

[61] Y. Yang, Z. Jia, Y. Wu, R.-C. Xiao, Z. H. Hang, H. Jiang, and X. C. Xie, Gapped topological kink states and topological corner states in honeycomb lattice, Sci. Bull. **65**, 531 (2020).

[62] M. Ziatdinov, H. Lim, S. Fujii, K. Kusakabe, M. Kiguchi, T. Enoki, and Y. Kim, Chemically induced topological zero mode at graphene armchair edges, Phys. Chem. Chem. Phys. **19**, 5145 (2017).

[63] L.-J. Shi, L.-Z. Yang, J.-Q. Deng, L.-H. Tong, Q. Wu, L. Zhang, L. Zhang, L.-J. Yin, and Z. Qin, Constructing graphene nanostructures with zigzag edge terminations by controllable STM tearing and folding, Carbon **165**, 169 (2020).

[64] B. Liu, P. Gong, Y. Sun, K. Ba, S. Xie, and Z. Sun, Precise lateral control of graphene via living zigzag edges, Carbon **167**, 718 (2020).

[65] C. W. Peterson, T. Li, W. A. Benalcazar, T. L. Hughes, and G. Bahl, A fractional corner anomaly reveals higher-order topology, Science **368**, 1114 (2020).

[66] C. W. Hsu, B. Zhen, A. D. Stone, J. D. Joannopoulos, and M. Soljačić, Bound states in the continuum, Nat. Rev. Mater. **1**, 16048 (2016).

[67] W. A. Benalcazar and A. Cerjan, Bound states in the continuum of higher-order topological insulators, Phys. Rev. B **101**, 161116(R) (2020).

[68] A. Cerjan, M. Jürgensen, W. A. Benalcazar, S. Mukherjee, and M. C. Rechtsman, Observation of a Higher-Order Topological Bound State in the Continuum, Phys. Rev. Lett. **125**, 213901 (2020).

[69] C. Yuce and H. Ramezani, Topological states in a non-hermitian two-dimensional Su-Schrieffer-Heeger model, Phys. Rev. A **100**, 032102 (2019).

[70] S. Debroy, S. Sivasubramani, G. Vaidya, S. G. Acharyya, and A. Acharyya, Temperature and size effect on the electrical properties of monolayer graphene based interconnects for next generation MQCA based nanoelectronics, Sci. Rep. **10**, 6240 (2020).

[71] C. Peng, R.-Q. He, and Z.-Y. Lu, Correlation effects in quadrupole insulators: A quantum Monte Carlo study, Phys. Rev. B **102**, 045110 (2020).

[72] F. D. M. Haldane, Model for a Quantum Hall Effect without Landau Levels: Condensed-Matter Realization of the "Parity Anomaly", Phys. Rev. Lett. **61**, 2015 (1988).

[73] C. L. Kane and E. J. Mele, Quantum Spin Hall Effect in Graphene, Phys. Rev. Lett. **95**, 226801 (2005).